Venus cloud top winds from tracking UV features in Venus Monitoring Camera images

R. Moissl,[1] I. Khatuntsev,[1,2] S. S. Limaye,[3] D. V. Titov,[1,2] W. J. Markiewicz,[1] N. I. Ignatiev,[2] T. Roatsch,[4] K.-D. Matz,[4] R. Jaumann,[4] M. Almeida,[5] G. Portyankina,[1] T. Behnke,[4] and S. F. Hviid[1]

Received 15 February 2008; revised 9 October 2008; accepted 10 November 2008; published 17 March 2009.

[1] To date dynamical observations of the Venus clouds have delivered mainly either only short-term or long-term averaged results. With the Venus Monitoring Camera (VMC) it finally became possible to investigate the global dynamics with a relatively high resolution in space and time on a long-term basis. Our findings from manual cloud feature wind tracking in VMC UV image sequences so far show that the details of the mesospheric dynamics of Venus appear to be highly variable. Although the general rotation of the atmosphere remained relatively stable since Mariner 10, more than 30 years ago, by now, there are indications of short-term variations in the general circulation pattern of the Venus atmosphere at cloud top level. In some cases, significant variations in the zonal wind properties occur on a timescale of days. In other cases, we see rather stable conditions over one atmospheric revolution, or longer, at cloud top level. It remains an interesting question whether the irregularly observed midlatitude jets are indeed variable or simply become shielded from view by higher H_2SO_4 haze layers for varying time intervals. Winds at latitudes higher than 60°S are still difficult to obtain track because of low contrast and scarcity of features but increasing data is being collected. Over all, it was possible to extend latitudinal coverage of the cloud top winds with VMC observations. Thermal tides seem to be present in the data, but final confirmation still depends on synthesis of Visible and Infrared Thermal Imaging Spectrometer and VMC observations on night and dayside. Although poorly resolved, meridional wind speed measurements agree mainly with previous observations and with the presence of a Hadley cell spanning between equatorial region and about 45°S latitude.

Citation: Moissl, R., et al. (2009), Venus cloud top winds from tracking UV features in Venus Monitoring Camera images, *J. Geophys. Res.*, *114*, E00B31, doi:10.1029/2008JE003117.

1. Introduction

[2] The cloud level super rotation of the atmosphere, first determined from ground based images [*Boyer and Guerin*, 1969] has been measured from Mariner 10 [*Limaye and Suomi*, 1981], Pioneer Venus and Galileo missions [*Rossow et al.*, 1990; *Belton et al.*, 1991; *Toigo et al.*, 1994; *Limaye*, 2007; *Peralta et al.*, 2007].

[3] During its flyby at Venus in 1974 Mariner 10 collected image data with resolutions down to 30 km/pixel during the 8 days around its closest approach to the planet. The most extensive data set so far was obtained by the Pioneer Venus OCPP instrument between 1979 and 1986. The Galileo probe, which performed a flyby in 1990, acquired data during the 16 h around closest approach to Venus. The UV filter was centered at a wavelength of 400 nm.

[4] The super rotation refers to the fact that bulk of the atmosphere of Venus rotates faster than the underlying solid planet from the surface to an altitude of ~80 km, reaching speeds above the visible cloud top at rates ~50 times faster than the planet. How this super rotation is maintained has been a puzzle since its discovery. The combination of the strong zonal flow and the weaker meridional flow explains the spiraling streaks seen in the ultraviolet images [*Suomi*, 1975; *Smith and Gierasch*, 1996] and is likely responsible for, or an artifact of the hemispheric vortex organization of the circulation centered over each pole of Venus [*Limaye and Suomi*, 1981; *Limaye*, 2007].

[5] The inferred global circulation is that the atmosphere is organized vertically in at least one Hadley circulation cell, wherein the solar heating in low latitudes causes rising motion and near the cloud level atmosphere flows toward the pole where radiative cooling leads to sinking to com-

[1]Max-Planck-Institut fuer Sonnensystemforschung, Katlenburg-Lindau, Germany.
[2]Space Research Institute, Moscow, Russia.
[3]Space Science and Engineering Center, University of Wisconsin-Madison, Madison, Wisconsin, USA.
[4]Institut fur Planetenforschung, Deutsches Zentrum fur Luft- und Raumfahrt, Berlin, Germany.
[5]European Space Astronomy Centre, European Space Agency, Madrid, Spain.

0148-0227/09/2008JE003117

plete the return flow (i.e., thermally direct circulation). The indirect evidence of this cell extending to the limiting altitude of the observations (~40 km) was determined from the detection of the solenoidal circulation from the temperature profiles determined from the radio occultation technique from the Pioneer Venus orbiter through the determination of the angle between the pressure and density surfaces [*Limaye*, 1985]. Winds inferred from tracking entry probes are inconclusive about whether there may be multiple cells between the surface and the 40 km level below which the thermal structure data from radio occultations are not available, but have been postulated [*Schubert*, 1983].

[6] The previous studies of the cloud motions have revealed aspects of the cloud level circulation such as Kelvin and gravity waves [*Del Genio and Rossow*, 1990; *Smith and Gierasch*, 1996] and presence of thermal tides [*Limaye et al.*, 1982; *Rossow et al.*, 1990; *Limaye*, 2007]. Investigations on these phenomena are part of the continuing effort to understand the processes that maintain the super rotation of the atmosphere [*Schubert*, 1983; *Schubert et al.*, 2007] These include observations of the circulation below the clouds from entry probes or balloons and, more recently, on the night side from tracking of features in near infrared observations of Venus from Galileo [*Carlson et al.*, 1991; *Sánchez-Lavega et al.*, 2008] and Venus Express as well as from telescopes on Earth [*Crisp et al.*, 1991; *Limaye et al.*, 1988].

[7] *Schubert* [1983] discusses the different suggestions for the maintenance of the super rotation of the atmosphere, which include processes such as equatorward transport of angular momentum by eddies and angular momentum transport through solar thermal tides. Thus much of the effort continues to be directed at establishing the roles of eddies and solar tides in the transport of angular momentum. *Limaye* [2007] discussed the challenges posed by the lack of sufficient and complete observations due to the fact that until recently the thermal tides in the winds could be detected only from the cloud motions measured on the day side, which likely introduced a bias in the estimates of meridional transport of angular momentum by the mean and eddy circulation if the night side wind distributions were strong and different enough to cause the true zonal average to be substantially different from the day side average. The absence of night side information also impacts the inferences about the Kelvin waves [*Del Genio and Rossow*, 1990] to some degree and in the understanding of true temporal variations in the cloud level circulation on Venus.

[8] One of the main goals of the Venus Express mission is to provide a global and systematic study of the atmospheric circulation [*Svedhem et al.*, 2007; *Titov et al.*, 2006]. We use sequences of UV images taken by Venus Monitoring Camera [*Markiewicz et al.*, 2007a, 2007b] to measure the wind speeds at the cloud tops by tracking apparent motions of the cloud features. In comparison to the earlier investigations these observations provide extended and systematic latitude and local time coverage including high latitudes in nadir viewing geometry, significantly better temporal resolution and long-term coverage, and have higher spatial resolution. The preliminary results of the UV digital cloud tracking were presented by *Markiewicz et al.* [2007b]. Here we describe in detail the Venus Monitoring Camera (VMC) imaging sequences, the cloud tracking techniques, and the results of cloud tracking in VMC images from two slightly different manual tracking techniques during the primary mission of Venus Express. The digital tracking results will be briefly addressed in this work and presented in more detail at a later date pending further analysis.

2. Observations and Data Set

[9] The Venus Monitoring Camera is a wide angle camera with a field of view of 17°, imaging Venus simultaneously in four narrow-band filter channels. All four channels are sharing one CCD detector, each one using one quadrant of the CCD. Two narrow band filters are in the near-IR (965 nm and 1010 nm), one in the visible (513 nm) and one in UV (365 nm). The UV channel is centered at the spectral signature of the unknown UV absorber. We use this filter to observe and track the UV cloud markings on the dayside, which are detected at around 70 km of altitude, where the optical depth in the UV approaches unity [*Tomasko et al.*, 1985; N. I. Ignatiev et al., Altimetry of the Venus cloud tops from the Venus Express observations, submitted to *Journal of Geophysical Research*, 2008]. A more detailed description of the VMC instrument, its properties and science goals has been presented in the work of *Markiewicz et al.* [2007a; 2007b].

[10] Because of the highly elliptical polar orbit of the Venus Express spacecraft the distance from the planet varies from ~250 km at pericenter to ~66.000 km in apocenter in the course of one 24 h orbit. Therefore the VMC angular resolution of 0.74 mrad per pixel translates into spatial resolution of approximately 0.2 km/pixel at pericenter and ~50 km/pixel around apocenter. Consequently, VMC data yields high-resolution close-up images of the Northern Hemisphere as well as a global view of Venus from the South Pole.

[11] In October 2007 Venus Express completed its primary mission [*Svedhem et al.*, 2007; *Titov et al.*, 2006]. In the course of 510 revolutions about the planet, the Venus Monitoring Camera acquired a total inventory of roughly 67,000 images with 31,800 in the UV among them. The data and results presented in this paper are based on the images obtained at 60,000–26,000 km distance from Venus, corresponding to a pixel size of 20–50 km. Typical time intervals between image pairs used for cloud tracking are ~40 min that corresponds to 5–10 pixel displacement of cloud features between the images. This selection is a compromise between the error in velocity measurements and temporal resolution. The planet coverage, regarding tracked UV markings, ranges from about 10°N to 80°S in latitude and 8–16 h local time. The contrast in VMC UV images varies between 5% and 30%, with typical values of 15–30% for the tracked features.

[12] Because of some minor damage to the detector due to solar irradiation, all images are subject to an in-flight flat fielding procedure before evaluation. In order to eliminate all artifacts in the VMC data, a series of images is acquired at high latitudes where the observed contrast is at a minimum. The images of these sequences are then averaged to achieve a uniformly gray background on which all persistent artifacts stand out prominently. All images in the corresponding orbit are then divided by the (normalized)

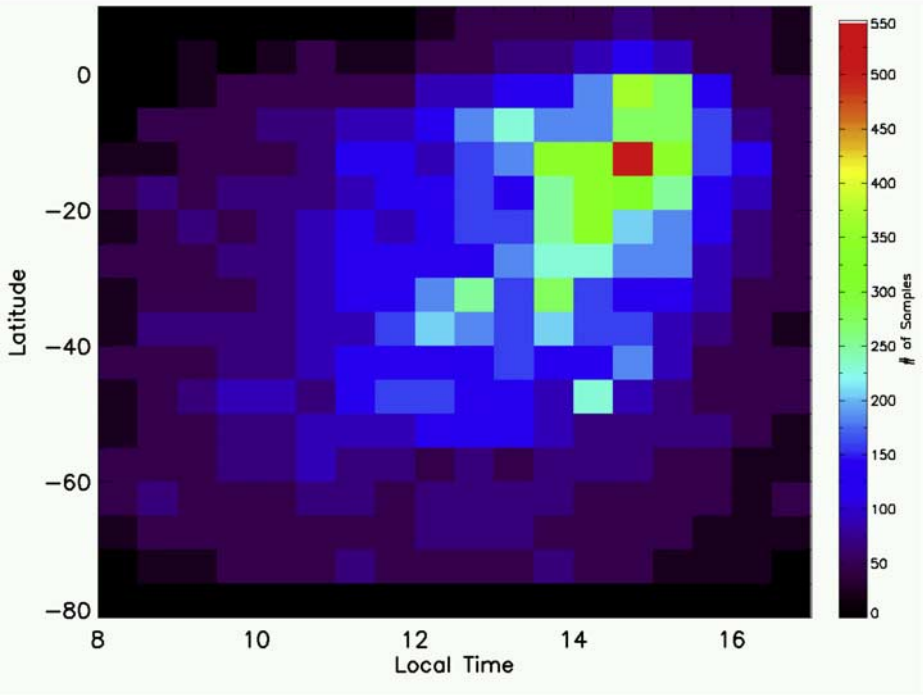

Figure 1. Coverage by VMC cloud-tracking measurements per 5° latitude × 0.5 h local time bin.

flat field. Because of a temporal evolution of some artifact patterns minor residuals may remain.

[13] The Venus Express orbit can be divided roughly into three parts: apocentric (66,000–50,000 km distance from the planet), ascending branch (50,000–10,000 km) and pericentric (10,000–250 km). In these three orbital segments VMC images are acquired in order to study various types of features and observe different aspects of the cloud top dynamics. In apocentric images Venus is seen almost directly from beneath the South Pole, so the polar region is imaged without any foreshortening (unlike previous missions), but the low latitudes are seen in oblique view. This part of the VMC data set is used to study near-polar global dynamics and cloud morphology. In the ascending branch VMC observes middle and low latitudes in nadir geometry. Local time coverage depends on the sub spacecraft longitude that slowly changes from one orbit to another (∼1.5 deg or 6 min per day). The ascending branch images are predominantly used to track winds from medium and small-scale features, ranging from about thousand down to several hundred kilometers in diameter. At close approach cloud features on scales down to few tens of kilometers in size can be identified in the images. However, at distances closer than 10,000 km wind tracking becomes increasingly more difficult as the rapid motion of the spacecraft decreases the overlap between images and features can be kept in the field of view only for short times.

[14] Figure 1 shows the coverage of the latitude-local-time field by the VMC cloud tracking. The number of vectors peaks near downstream (to the west) of the sub solar region where a large number of discrete features of convective nature is regularly observed and drops toward higher latitudes as well as the morning and evening terminator. The main limiting factor for coverage in local time in the dusk and dawn regions are the steep brightness gradients which, even in high-pass-filtered images, dampen contrast of the UV markings. At polar latitudes the morphology of the clouds is different altogether, presumably due to a decrease in or even absence of convective activity and presence of submicron haze [*Kawabata et al.*, 1980]. This results in lack of discrete features, very low contrasts and drawn-out diffuse feature boundaries. In total, about 20,000 vectors have been extracted from ∼450 image pairs.

[15] During the primary mission the descending branch of the Venus Express orbit was reserved for data transmission to Earth. In conjunction with the relative change in local solar time of the orbit plane, this lead to separation of the VMC wind tracking data into three periods in which it was possible to observe the dayside of Venus in ascending branch from a sufficient distance. These three periods are separated by gaps of almost 140 orbits in which VMC was pointed either to the night side or too close to the terminator to allow for tracking sequences to be taken in the required orbit segment. The first period spans from orbit 29 to 72 (containing tracking sequences from orbits 29, 30, 31, 34, 38, 46, 51, 56, 60, 61, 72, May–June 2006), the second period from orbit 208 to 295 (containing 208, 210, 230, 246, 250, 257, 258, 260, 263, 265–267, 279, 281–284, 295, November 2006 to January 2007), the third period from orbit 439 to 530 (containing 439, 440, 442, 453, 460–463, 469, 471, 530, July–September 2007). Table 1 is listing the according dates of each orbit in the data set, together with the approximate coverage of the wind tracking in local time (LTR) and latitude (LAR), as well as the local time of the subspacecraft point at ascending node (LTAN).

[16] Usually the individual wind tracking sequences are separated from each other by several days. But also sets of up to 4 consecutive orbits are present in the data set. These

Table 1. List of All Orbits in the Data Set[a]

Orbit	Date	LTR (h)	LAR (°)	LTAN (h)
29	19 May 2006	10.0–15.1	−78 to −15	13.6
30	20 May 2006	08.8–16.5	−78–01	13.7
31	21 May 2006	09.3–16.7	−76–13	13.8
34	24 May 2006	08.2–16.2	−79 to −02	14.1
38	28 May 2006	08.9–15.5	−65–05	14.6
46	5 Jun. 2006	08.1–15.8	−81–05	15.4
51	10 Jun. 2006	09.3–15.6	−79 to −02	15.9
56	15 Jun. 2006	10.1–16.7	−69–00	16.5
60	19 Jun. 2006	09.4–16.4	−73–07	16.9
61	20 Jun. 2006	11.5–16.3	−67–12	17.0
72	1 Jul. 2006	09.7–17.4	−74–02	18.2
208	15 Nov. 2006	07.8–15.4	−73–04	8.8
210	17 Nov. 2006	07.8–14.6	−75–05	9.0
230	7 Dec. 2006	08.0–15.3	−73–04	11.2
246	23 Dec. 2006	08.0–16.3	−71–08	12.8
250	27 Dec. 2006	07.8–16.0	−78–09	13.3
257	3 Jan. 2007	08.6–16.3	−67–11	14.0
258	4 Jan. 2007	08.8–15.8	−75–07	14.1
260	6 Jan. 2007	08.1–16.4	−76–05	14.3
263	9 Jan. 2007	08.3–16.6	−77–11	14.6
265	11 Jan. 2007	09.9–16.3	−75–10	14.8
266	12 Jan. 2007	08.6–16.3	−72–15	14.9
267	13 Jan. 2007	10.6–16.4	−73–06	15.0
279	25 Jan. 2007	07.9–17.2	−82–08	16.3
281	27 Jan. 2007	09.5–17.2	−73–11	16.5
282	28 Jan. 2007	08.5–17.2	−84–13	16.6
283	29 Jan. 2007	09.0–17.0	−77 to −06	16.7
284	30 Jan. 2007	10.3–16.8	−76–07	16.8
295	10 Feb. 2007	09.6–17.0	−80–01	18.0
439	4 Jul. 2007	08.2–15.3	−78 to −02	9.5
440	5 Jul. 2007	08.2–16.1	−80–01	9.6
442	7 Jul. 2007	07.6–15.2	−79–00	9.8
453	18 Jul. 2007	07.1–16.7	−82–01	11.0
460	25 Jul. 2007	07.3–15.9	−74–04	11.7
461	26 Jul. 2007	08.6–15.8	−72 to −02	11.8
462	27 Jul. 2007	08.0–16.7	−73–06	11.9
463	28 Jul. 2007	07.4–16.7	−74–01	12.0
469	3 Aug. 2007	07.6–16.3	−74–08	12.7
471	4 Aug. 2007	07.8–16.7	−75–03	12.9
530	2 Oct. 2007	08.9–17.2	−74 to −03	19.1

[a]The LTR column shows the approximate coverage of the wind tracking in local time (decimal representation). The LAR column gives approximate latitudinal coverage (negative values denote southern latitudes). LTAN refers to the subspacecraft local time at ascending node.

small irregularities in coverage were compensated by the fact that the field of view included broad range of local times in distant imaging.

3. Wind Tracking Procedures

3.1. Description of the Employed Tracking Methods

[17] We used both digital (automatic) and visual (manual) tracking of the UV cloud markings to derive the wind speeds. Three independent experimenters used imaging sequences from 39 orbits and applied two different visual tracking techniques and automatic wind tracking software. The first step in all cloud tracking methods was to establish navigation for the used images. We used the postprocessed SPICE data (see: http://naif.jpl.nasa.gov/naif/) to calculate VMC boresight vectors and their intersection with the cloud layer, assigning planetary coordinates to each image pixel. The cloud top height was set to a fixed value of 70 km above the planetary surface for navigation purposes. We expect the actual cloud top height to vary by about ±5 km around this level, which results in negligible uncertainties in coordinate determination.

[18] For historical reasons and software availability we use two different procedures for visual wind speed measurements. The "sequential method" traces back to the wind speed measurements from previous missions, especially from Pioneer Venus OCPP observations [*Limaye*, 1988; *Limaye et al.*, 1982, 1988]. As done for the OCPP wind speed measurements a loop of an entire image sequence from one VEX orbit was displayed in either equiangular (rectilinear, 0.2°/pixel) or polar projection onto a fixed coordinate grid (Figure 2 (right)). In this method motion of a cloud marking is observed in the way of a short movie clip, giving the experimenter an overview of the path of a selected cloud feature as well as the global pattern of motion. After familiarizing with the general flow pattern the experimenter puts small markers on distinctive cloud features in one image from the given orbit. Then the loop is continued, switching to a later image from the same sequence. There, another group of markers is put on the same cloud features. These steps are then repeated until the selected cloud features have changed significantly from their initial shapes and sizes and cannot be identified anymore. To enhance visibility of the cloud features a contrast enhancing high pass filter had been applied to the images after care was taken that the filtering did not alter any other image properties. This technique was used by two observers for about 40% (∼8000) cloud vectors.

[19] The "paired method" is a straightforward approach in which two different images from the same sequence are displayed side by side on a monitor and the cloud features in both are observed and compared simultaneously (Figure 2 (left and middle)). Also in this method, markers are set in order to track the corresponding points of cloud features in the compared image pairs. One significant difference is that here the images did not undergo any filtering, contrast enhancement or projection. Thus, basically unaltered VMC images were used for tracking with this method. The images were only slightly resized in order to achieve an approximately constant display size of the planet in each image. The paired method was used by one observer for about 60% (∼12,000) of cloud vectors.

[20] Although the basic principle, visual correlation between two images, is the same in both approaches, there are subtle but important differences. In the first case the observer tracks clouds by blink comparison between two images, trying to follow displacement of the tracked features on the fixed coordinate grid. In the second case the tracked feature is seen in both images simultaneously, thus emphasizing visual pattern recognition.

[21] In both methods the experimenters tracked a great variety of feature types. Basically all features that did not span on a globally significant scale were used to track the cloud movements. We did not differentiate between "bright" and "dark" features, tracking both alike. The main criteria for feature selection were as follows: (1) Significant, well discernible contrast between the feature and its immediate surroundings. No fixed criterion was applied but the vast majority of tracked features had contrasts in excess of 15 % with respect to their surrounding. (2) Features size of 100–300 km that allows for reliable identification of the feature center (only in equatorial regions). (3) Prominent

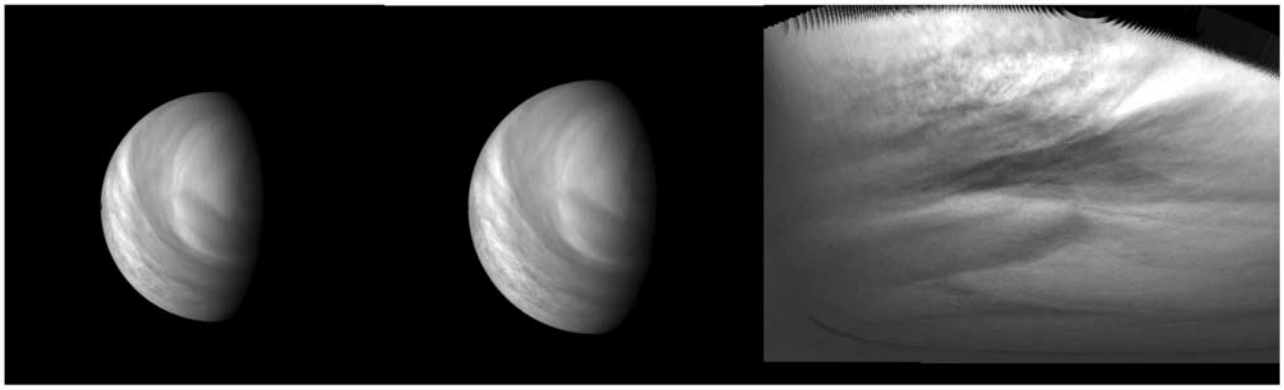

Figure 2. Typical VMC UV images used for tracking purposes. (left and middle) Pair of original VMC images used in the paired method. (right) Image in rectilinear projection used in sequential method.

shapes like protrusions or clearly edged parts of boundaries for larger features. (4) Minimum time intervals between images were chosen to allow for resolving wind speed differences of about 10–20 m/s (depending on image resolution). (5) No features from the limb regions were used because they are subject to foreshortening.

[22] The wind speeds in both methods were derived in similar ways. First the navigation data was linked to the images (for both, the projected and unprojected images). Then latitude and longitude of the respective marked pixels were extracted for all measurements of the sequence. From these values and the time intervals between images the zonal and meridional cloud speeds were calculated as

$$U(\lambda, t, \varphi) = \Delta\lambda R_C/\Delta t \cos(\varphi);\ V(\varphi, t) = \Delta\varphi R_C/\Delta t,$$

where U and V are zonal and meridional wind speed components, λ and φ are longitude and latitude, R_C is the distance from the planetary center to 70 km above the surface (R_C = 6121.8 km), and Δt is the time between images.

[23] For the digital tracking in VMC images we used the same algorithm as applied by *Rossow et al.* [1990]. The analysis was performed systematically in pairs of images with at least one hour time difference using cross correlation as a metric with a "cloud" target of 10 × 10 pixels in the first image (2° × 2° latitude by longitude). The displacement between the target location in the first image and the location of the maximum cross correlation coefficient in the second image between the search and the target was taken as the best estimate of the movement of the selected target over the interval between both images. The displacement over the two images leads to the determination of the zonal and meridional components of the cloud level flow. The search window in pixels was set to a window equivalent to a maximum flow of ±100 m/s in the meridional and −200 m/s in the zonal direction, accounting for the time interval between the images. Here the digital tracking results on ~205,000 vectors obtained from images acquired on nine orbits (30, 31, 34, 38, 46, 51, 56, 60, and 61) are presented in Figure 3 to show the generally good agreement between the results from visual and digital tracking. Preliminary results from orbits 262–267 were presented by *Markiewicz et al.* [2007b].

[24] Figure 2 shows examples of images used in the two different visual tracking methods. After the tracking sequences have been compiled from the orbital data set and markers have been set, the marker positions are determined and recorded. From the resulting set of vectors, latitudinal and/or longitudinal wind profiles and maps can be determined, by averaging all wind vectors inside a latitude bin. From the average density of retrieved vectors per orbit, we decided to use latitude bins of 5° and longitude bins of 7.5° (corresponding to 0.5 h of local solar time) in order to maintain good levels of statistics.

3.2. Comparison of Wind Tracking Measurements

[25] As is obvious from Figure 2, the appearance of the cloud deck strongly differs between the original and the projected images. While the original images show all parts of the planet true to the perspective of the VMC, the rectilinear projection tends to distort the polar region quite drastically. Respectively, the polar projection distorts the equatorial region to a point where features get too distorted to be used for tracking. The basic properties of both methods will be addressed below.

[26] Since Venus cloud features evolve over time, visual tracking relies on a somewhat subjective approach to identify a cloud feature in two or more images acquired at different times. In the case of VMC data, the orbital motion of the Venus Express spacecraft results in a slightly different "view" of a given cloud because of both its displacement due to ambient flow and due to the change in perspective. The paired method thus visually measures the combined displacement from perspective and ambient flow. And the part due to perspective change is accounted for by the image navigation implicitly. From the preserved perspective in the original images, the experimenter has good insight into which parts are seen heavily foreshortened, especially close to the limbs. This allows for a well founded possibility to select only the weakly or nonforeshortened features for tracking. On the other hand the apparent feature size and resolution change along the orbit. Therefore one has to be careful about reidentifying the same part of a feature in different images. This is especially the case in the low-contrast areas at higher latitudes. There it is possible for faint feature boundaries to interfere with so-called "flat field

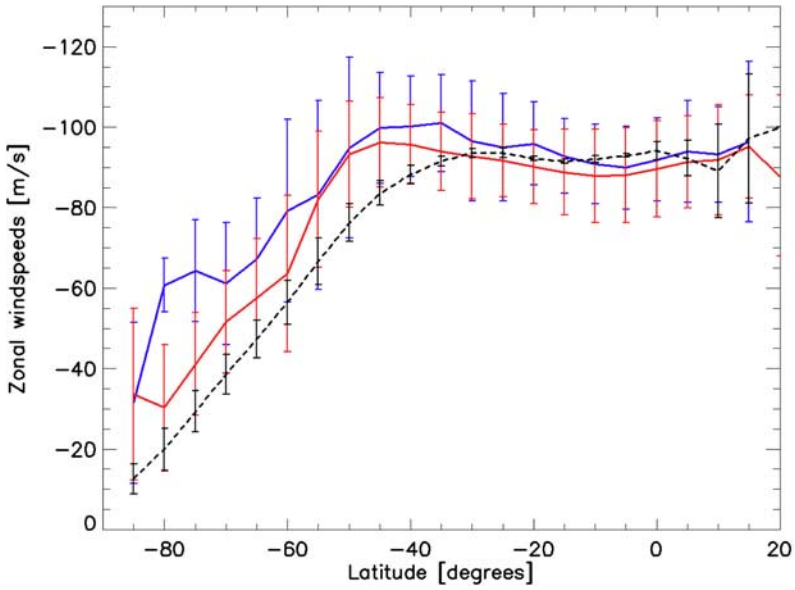

Figure 3. Latitude profiles of zonal winds derived from the paired (red line) tracking, sequential (blue line) visual tracking, and digital (black line) tracking. Error bars represent standard deviation due to uncertainties of individual measurements.

remainders'' which result from the flat field correction process applied to VMC images.

[27] In the sequential tracking method the flat field remainders become distinctively visible after high pass filtering, because they represent high-frequency variations. So they can be easily identified and avoided, since their apparent movement is governed by the change of the VMC perspective on the planet. Thus they mimic a movement completely different from all real atmospheric flows.

[28] Figure 3 compares the latitude profiles, averaged in 5° latitude bins, of zonal wind speeds derived from the agglomerate data sets of the sequential (red curve) and paired (blue curve) visual tracking methods and those from digital tracking (black curve). The sequential method shows slightly higher speeds on average, which might be an indication for minimal bias due to either method. The biggest differences occur at high latitudes, between 70 and 80°S. Although the two methods do not actually agree there very well within their respective measurement accuracies, this is more likely due to the difficulties in finding adequate features for tracking in these latitudes than to differences in the tracking methods. Therefore, these deviations seem to originate from observer bias. Regarding the above mentioned risk of interference of faint, streaky cloud features with flat field remainders, some influence of this interference might possibly also play a role in this. Also the digital and the visual tracking results from the VMC data are in very good agreement up to about 40° latitude, and show a difference of ∼15 or 20 ms^{-1} between 40 and 60° latitude from the visual tracking. There are likely two causes for this (1) the morphology and low contrast at these latitudes makes pattern matching by digital cross correlation difficult and (2) a selection effect in that visually only the targets that are moving fast are discernible, but in longitude regions where the flow may be slower, no targets are seen as is suggested by the longitudinal distribution of the visual vectors. The digital results south of 60°S are not very reliable yet and are therefore to be viewed as entirely preliminary at this point.

[29] Further, the average standard variation in all latitude bins is approximately the same for both visual tracking methods. This is a clear indication that measurement accuracy is nearly the same for both methods.

[30] In conclusion, the deviations between the two visual methods are well on the order of the expected measurement uncertainty for single measurements in the according latitude regions. Despite the obvious discrepancy in the 70–80°S latitude range between the two profiles from the two visual tracking methods, we decided that merging also these results will improve the poor statistics in this region and minimize observer bias. From this we conclude that the results from both methods are in reasonable agreement to allow for regarding all measured wind vectors as one data set, regardless of the employed method. In consequence later on in the paper we do not differentiate the results by tracking method.

3.3. Error Sources and Systematic Uncertainties

[31] A number of measurement properties are influencing the accuracy of the wind speed measurements. Main sources of uncertainty are image resolution, measurement accuracy and feature evolution. Additionally some bias from the different methods and/or observers might introduce systematic errors.

[32] Velocity uncertainty of an individual measurement due to technical limitations, such as image resolution and

marker position error in the image is easily assessed via first-order Taylor expansion as follows:

$$\delta U = \sqrt{(\sqrt{2}R_c\delta\alpha\cos(\varphi)/\Delta t)^2 + (\delta\alpha R_C\sin(\varphi)/\Delta t)^2 + (\alpha\delta R_c\cos(\varphi)/\Delta t)^2}$$

$$\delta V = \sqrt{(\sqrt{2}R_c\delta\alpha/\Delta t)^2 + (\alpha\delta R_c/\Delta t)^2},$$

where δ values denominate total uncertainties for velocities (U,V), measured angular differences (α), and distance from Venus center to the cloud top (R_C) and φ is the latitude at measuring point.

[33] For equatorial latitudes the first term, assuming a 1 pixel error (corresponding to approximately 0.2–0.4° in latitude and longitude, depending on observing distance) and 40 min between images further away and 20 min when closing in, ranges from about 36 m/s at apocenter to roughly 10 m/s at 30,000 km distance from the planet, being 20 m/s on average. At higher latitudes the accuracy in latitudinal direction decreases further because of the convergence of latitude circles. This accuracy limit poses a great problem for deriving reliable meridional speeds, since they are supposed to be of the order of 10 m/s. Of course this source of uncertainty could be further suppressed through choice of image pairs with further increased time intervals. The early tracking sequences where too short to allow for reasonable statistics with image pairs separated by more than one hour, thus the chosen time intervals represent a trade-off between statistics and precision of the measurements. The second term, assuming 3–5 pixels between images and 10 km uncertainty in cloud deck height, remains well below 1 m/s in any case and can therefore be neglected.

[34] Sources for uncertainty of an individual measurement could arise from the following:

[35] 1. Pointing and mapping inaccuracies are considered to be negligible since both have proven to be extremely accurate and stable. A very conservative estimate would be an inaccuracy amounting to one pixel.

[36] 2. Pixelation and noise are assumed to amount to an error of one pixel if physical feature boundaries lie close to the edge of a pixel. Depending on flat field quality, which is varying from orbit to orbit since images of nearly featureless cloud areas are needed, the uncertainty by noise can reach up to two pixels.

[37] 3. Morphology and morphological evolution also influence the measurement accuracy. Since cloud features seldom have clear boundaries, there is always some possible (and variable) inaccuracy in determining the center or exact boundary line of a tracked feature. Furthermore, evolution of cloud features is observed, but because of time intervals between images being always smaller than 4 h, no significant inaccuracy should arise from them. This has been discussed already for the Pioneer Venus OCPP data set [*Rossow et al.*, 1990]. These issues are especially valid for higher latitudes, since the low contrasts there make identification of the feature boundaries more difficult. It is difficult to quantify the influence of these morphological uncertainties, since they vary significantly with latitude and feature type. As a rule of thumb, the corresponding uncertainty varies between one pixel for small, sharply pronounced features and up to three pixels for fuzzy low-contrast features in high latitudes.

[38] 4. Systematic and random errors from measurement methods are likely to have some effect, as mentioned above. To minimize the effects of erroneous wind speeds from faulty measurements, we decided to reject all vectors outside the interval of −160–0 m/s. The constraints for meridional wind speeds were −60–+60 m/s. These selection criteria lead to rejection of about 1.4% of all measured vectors.

[39] As in previous works about cloud top winds inferred from the cloud feature tracking, we find that the variability in the derived and the averaged wind speed profiles are larger than the expected uncertainties from individual measurements. Therefore we chose to apply the standard deviation of wind speeds in one latitude bin as a measure of uncertainty for all wind speed profiles.

4. Results of the Wind Tracking

4.1. Zonal Wind Profiles

[40] Figure 4 shows the averaged latitude profiles of zonal wind speed for the aggregate visual and digital tracking data sets, binned in latitude bins of 5° width. Also shown in Figure 4 is the profile obtained from the Visible and Infrared Thermal Imaging Spectrometer (VIRTIS) 380 nm channel data [*Sánchez-Lavega et al.*, 2008] and the corresponding rotation period derived from the digital and visual profiles. UV winds derived from both experiments are in good agreement although VIRTIS tends to show systematically stronger winds by ∼10 m/s. At low latitudes, zonal wind speed is 85–90 m/s and almost constant with latitude. The latitude profile shows a gradual increase to 100 m/s, peaked at ∼45°S, indicating the presence of a weak midlatitude jet which is also seen in the inferences from the VIRTIS thermal wind analysis [*Piccialli et al.*, 2008]. South of this latitude the wind speeds steadily decrease toward the pole. Although the profile is close to a solid body rotation curve at first glance, a closer look on the rotation period in Figure 4b reveals significant differences, where solid body rotation profiles would show up as horizontal lines. The kink at ∼10°N in the zonal wind profile is very likely an artifact, due to the rather poor sampling as it is at the very edge of VMC coverage of Venus in the tracking image sequences.

[41] The error bars represent standard deviation of the zonal wind speed in each latitude bin. The deviation increases toward higher latitudes, mostly due to the changes in morphology and difficulties in finding well defined UV markings there, as discussed above. The standard deviations exceed the uncertainties of individual measurements orbit (compare to Figure 3), indicating a likely orbit to orbit variability of the latitudinal profiles of the zonal wind component. Also variability with local time is likely to be present because of influences from planetary-scale waves [*Del Genio and Rossow*, 1990].

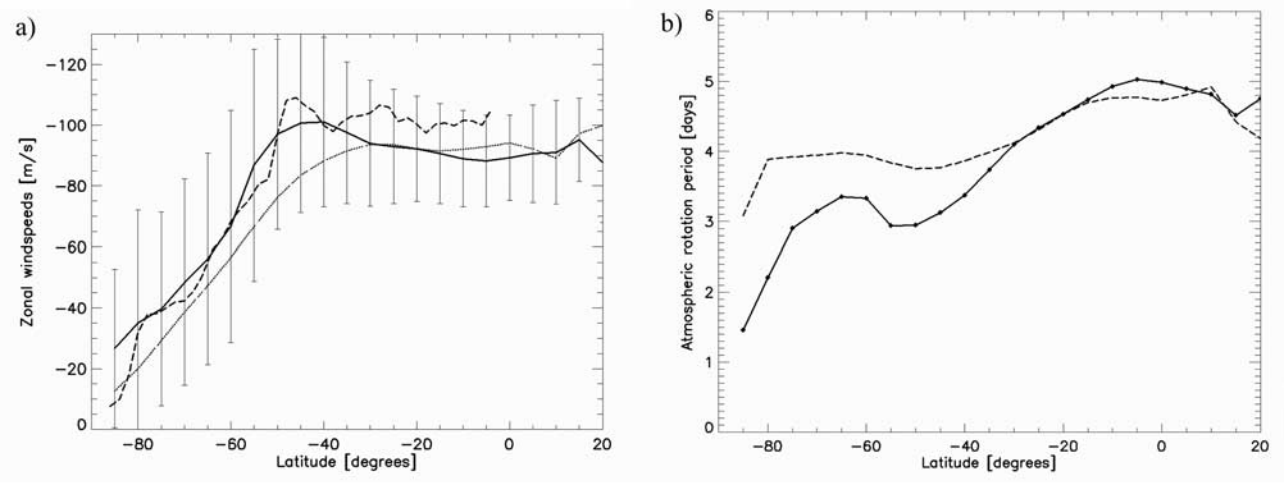

Figure 4. (a) Average zonal wind speed profiles from VMC visual (solid line) and digital (dotted line) in comparison with data from VIRTIS (dashed line) [*Sánchez-Lavega et al.*, 2008]. VMC and VIRTIS data is binned by 5° and 2°, respectively. The error bars represent standard deviation of the whole data set, including both measurement inaccuracies and orbit-by-orbit variations. (b) Corresponding rotation period profile from VMC wind tracking data (solid line is visual and dashed line is digital).

[42] Figure 5 shows a selection of different single orbit profiles and the average profiles for each of the three observation periods. Standard deviations per latitude bin divided by the respective square root of the number of measurements are shown in the bottom Figures 5a and 5b, giving a measure of the standard error for the average value per bin. The mean zonal speeds can change by as much as ~30 m/s from orbit to orbit and show significant variability in strength, position and even presence of the mid latitude wind speed maximum. Since these differences are well outside the standard error, they are most likely representing true variations of the zonal flow. These rather strong short-term variations in the wind speed profiles leads to slightly different characteristics in the average profiles for each of the three observation periods. In periods 1 and 3, pronounced wind speed maxima have been observed in the mid latitude regions, which is not the case for period 2.

4.2. Meridional Wind Component

[43] Since the measured tracking sequences do not allow for individual measurements with accuracies better than ±10 m/s, all results on the meridional winds have to be considered preliminary. The standard deviation in each 5° latitude bin amounts to ±13 m/s. These are about as large as the uncertainties expected to arise from the chosen combination of image resolutions and time intervals. This indicates that measurement inaccuracies are likely larger than the real variability in meridional wind speeds. Better accuracy meridional component profiles are possible from extended mission data and will be published in future.

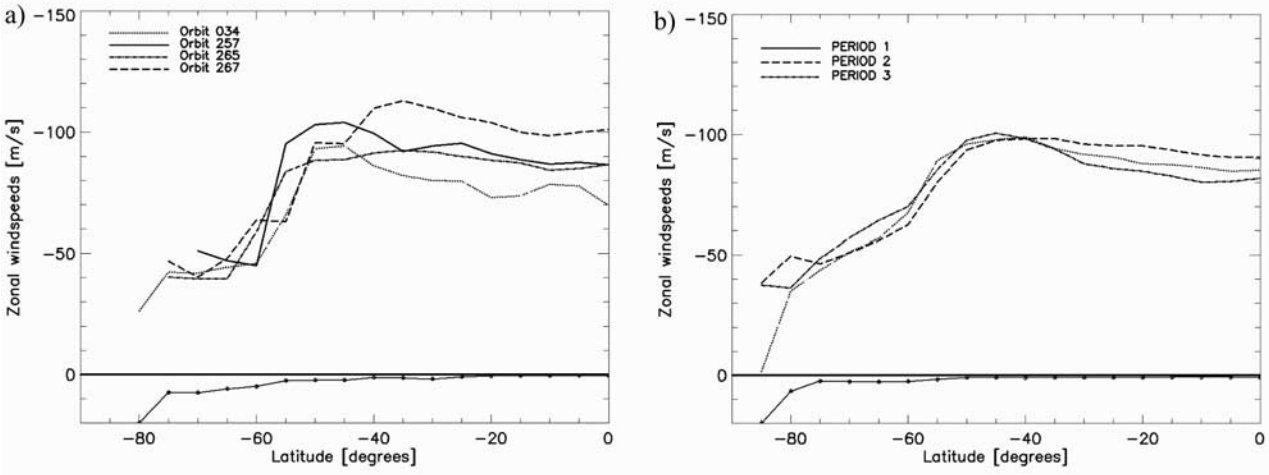

Figure 5. Latitude profiles of zonal wind for (a) individual orbits and (b) means for three tracking periods. The lines in the bottom of the images show average standard deviation divided by the square root of the number of measurements of the compared profiles for each latitude bin.

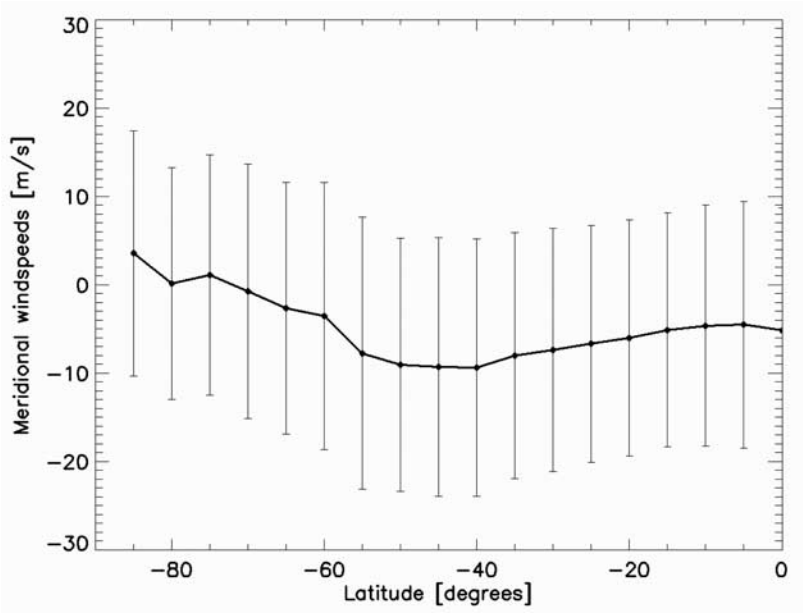

Figure 6. Average meridional wind profile. Error bars represent RMS deviation of measurements in one bin.

[44] As one can see from Figure 6 the average meridional wind component ranges from 0 to −10 m/s, which is roughly consistent with previous results. Meridional speeds are slightly increasing from about −5 m/s at the equator to peak values of ∼−10 m/s at mid latitudes between 40 and 55°S and then decreasing again toward the pole. The observed profile is in agreement with the assumption of a Hadley cell circulation between the equator and the mid latitudes [*Schubert*, 1983; *Gierasch et al.*, 1997].

[45] Future tracking sequences acquired at shorter distances from Venus will help to improve on accuracy of the meridional wind measurements by increasing image resolution which until now is not sufficient to satisfactory resolve wind speeds on the order of 0–10 m/s. We hope to be able to investigate temporal variability once higher-resolution tracking sequences have been evaluated.

4.3. Dependence of the Zonal Component on Local Solar Time

[46] Figure 7 shows the average zonal wind field as a function of latitude and local time after binning the wind speed vectors in "boxes" of 0.5 h local solar

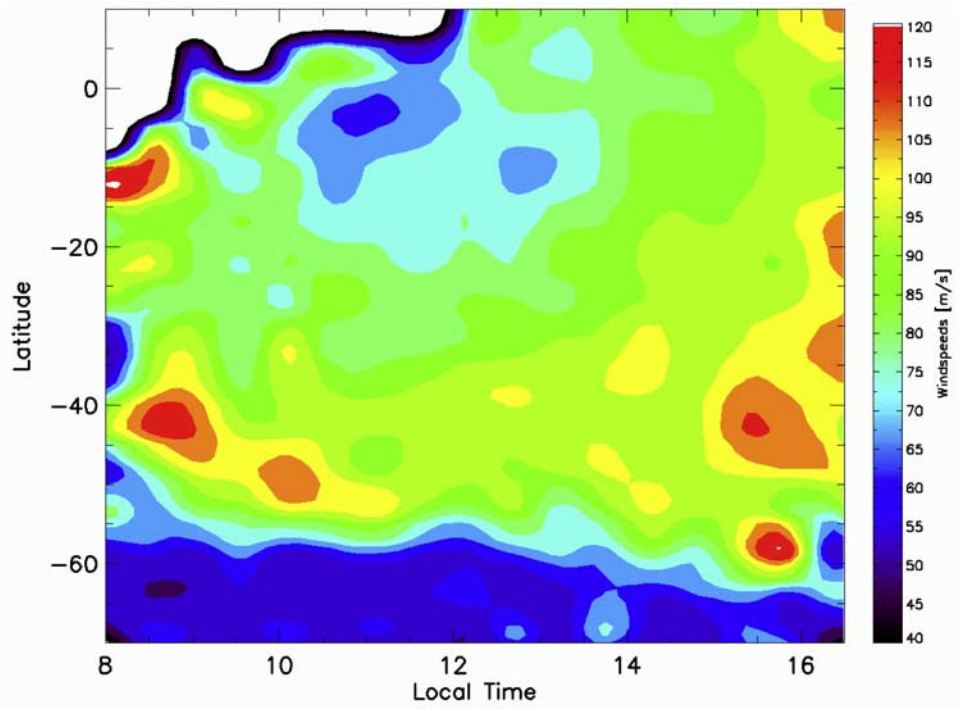

Figure 7. Local solar time versus latitude field of the zonal wind in the Southern Hemisphere.

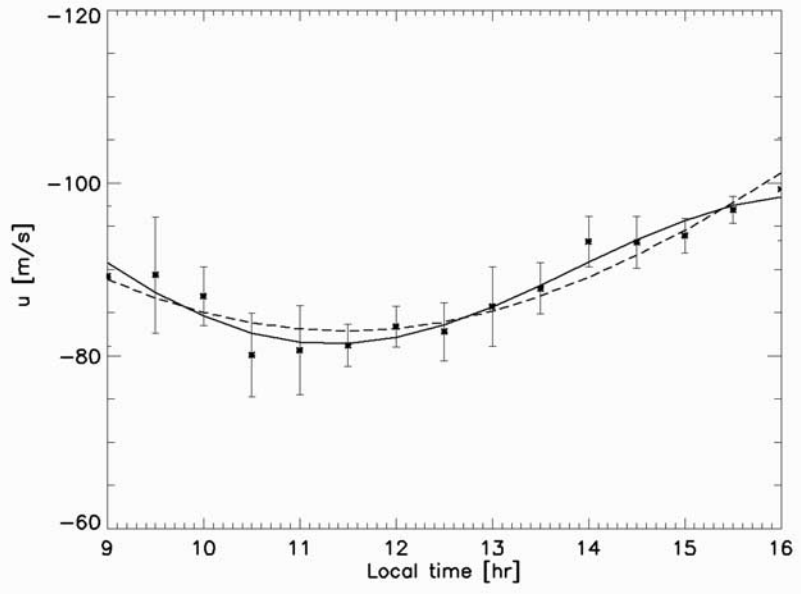

Figure 8. Local time profile of average zonal wind speeds between 0 and 20°S. VMC measurements in comparison with best fit for diurnal and semidiurnal tidal model (solid line) and diurnal model only (dashed line).

time × 5° ltitude each. The zonal wind field has a pronounced minimum at ∼11.5 h slightly upstream of the subsolar point and accelerates in the afternoon in low latitudes. In the middle latitudes velocities are higher on average over the whole observed local time range and show less local time variability. In higher latitudes an increase in speed with local time is apparent down to 60°S. Toward the pole zonal speeds are decreasing rapidly.

[47] The data displayed in the Figure 7 has been divided into three latitude bands (0–20°S, 20–40°S, and 40–60°S) in order to evaluate tidal components in the zonal wind field in the different latitude regions (Figures 8, 9, and 10). In each of the latitude bands we compared the local time profiles to a tidal model that includes both diurnal and semidiurnal components

$$U(\lambda) = U_0 + U_1 \sin(\lambda + \Phi_1) + U_2 \sin(2\lambda + \Phi_2),$$

where U_0 is the zonal mean value, λ is the longitude, U_1 and U_2 are the diurnal and semidiurnal velocity amplitudes, and Φ_1 and Φ_2 are the diurnal and semidiurnal phase angles.

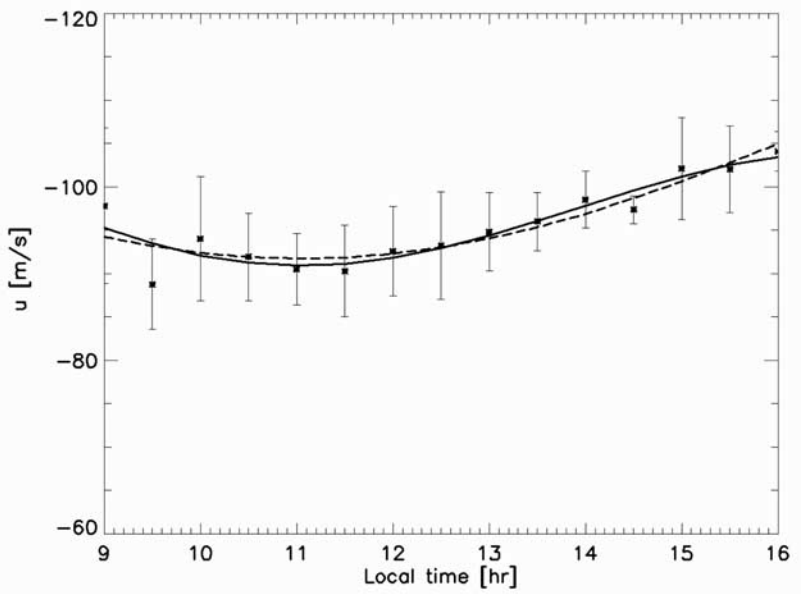

Figure 9. Local time profile of average zonal wind speeds between 20 and 40°S. VMC measurements in comparison with best fit for diurnal and semidiurnal tidal model (solid line) and diurnal model only (dashed line).

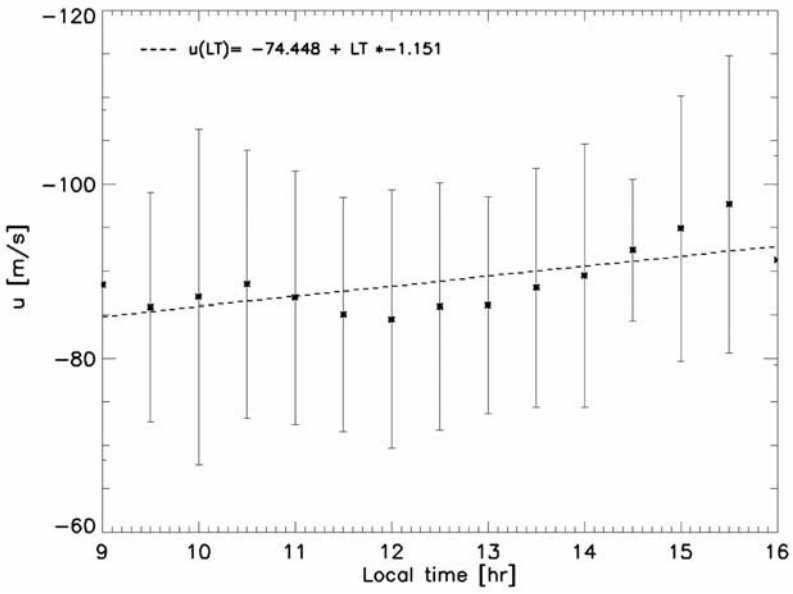

Figure 10. Local time profile of average zonal wind speeds between 40 and 60°S. The dashed line indicates the general trend with local time.

[48] In Figure 8, the local-time-dependent zonal wind component in the latitude strip between 0 and 20°S is being compared to fits from the diurnal-only part of the model and both diurnal and semidiurnal. Both fit curves show considerable agreement with the observed wind speeds, with higher agreement when both tidal wave modes are employed. Figure 9 shows the same comparison for the 20–40°S latitude strip. Here the data is in about equal agreement with both model curves. For the high-latitude region no conclusive correlation for diurnal and semidiurnal wave models could be obtained. The data shows, however, an overall trend toward increased wind speeds in the afternoon hours.

[49] In summary the observed local time variations of the zonal wind component is indicating the presence of solar thermal tides in VMC observations. Since only about 8 h of local time are covered from VMC measurements no reliable coefficients can be obtained from the employed model at this moment. We are continuing our efforts to expand the local time coverage of our tracking results to regions closer to the terminator regions.

5. Discussion and Conclusions

[50] Figure 11 shows a comparison between zonal wind speed profiles from VMC with previous observations from Pioneer Venus and Galileo. Although maximum resolutions of Mariner 10 Images lie within the same range as VMC data, lack of sufficient overlap with required time interval prevented measurements from the high-resolution images. Therefore we did not include results from Mariner 10 wind tracking in this comparison.

[51] The Pioneer Venus profile represents an average of the results from 1980 and 1982 imaging seasons of the OCPP polarimeter [*Limaye*, 2007] which is in good agreement with the VMC profile. The general shape of the Pioneer Venus orbit was quite similar to the one of Venus Express, with a pericenter at about 15°N the planet was observed mainly from a near-equatorial perspective. In contrast to the Pioneer Venus orbit, the 80°N pericenter of Venus Express allows VMC to deliver improved coverage of the Southern Hemisphere in nadir geometry. The average resolution of the OCPP images used for cloud tracking also lies around 30 km/pixel. One significant limitation of the OCPP image data is the 4 h time interval between images [*Rossow et al.*, 1980, 1990]. Whereas the instantaneous image acquisition of VMC allows for arbitrary intervals between images.

[52] Also the results from the high-resolution cloud tracking in Galileo images are in good general agreement with our findings. Prior to the VMC observations the Galileo images comprised the best resolved (down to 15 km/pixel) sequences used for cloud tracking and have recently been reused for high-resolution wind tracking [*Toigo et al.*, 1994; *Peralta et al.*, 2007]. Time intervals between Galileo images range from 15 min to 2 h, thus having in principle the same temporal resolution as the VMC sequences.

[53] So far, dynamical observations of the Venus clouds have delivered either only highly resolved short-term or broadly averaged long-term results. With VMC it finally became possible to investigate the global dynamics with a relatively high resolution in space and time on a long-term basis. Our findings from manual wind tracking in VMC UV image sequences so far show that the details of the cloud top level dynamics of Venus appear to be highly variable, down to a timescale of days. On the other side the average general rotation of the atmosphere remained effectively stable since Mariner 10, especially with regard to the remarkable agreement between VMC measurements and results from previous missions.

[54] In some cases significant variations in the zonal wind properties were observed especially in the mid latitude regions on an orbit to orbit basis, indicating possible

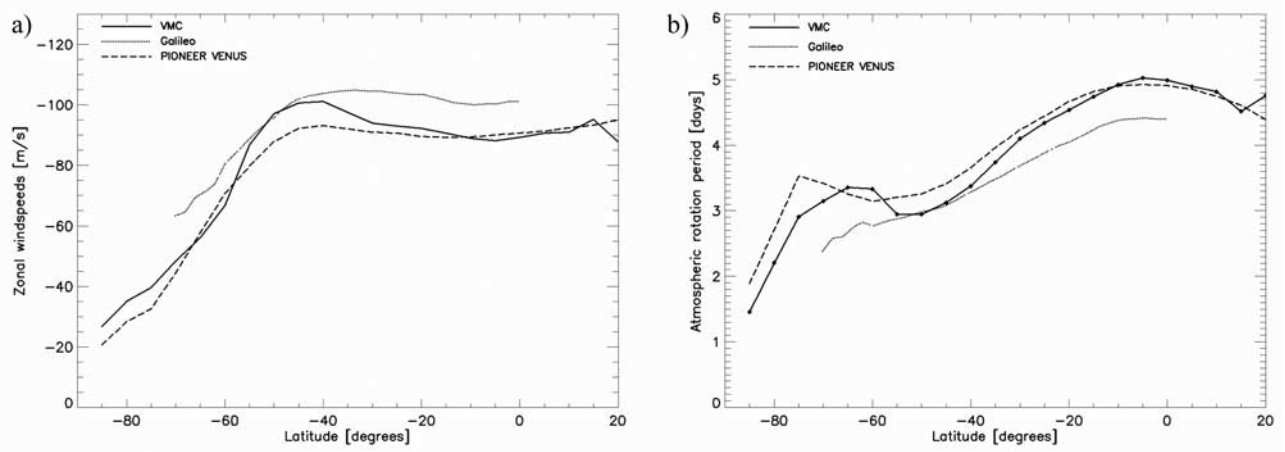

Figure 11. (a) Comparison of zonal wind speed profiles from VMC, Pioneer Venus, and Galileo measurements. (b) Corresponding rotation periods.

influences from global-scale wave modes. In other cases we measured more constant conditions over one atmospheric revolution or even longer periods, at cloud top level. These short-term variations between results from individual orbit tracking sequences appear to have an impact on the average zonal wind component profiles over longer-term observation periods. So far the search for Kelvin gravity wave modes in the consecutive measurements from orbits 281–284 and 460–463 did not yield any conclusive results. Most likely longer sequences of coherent tracking data will be required for clear identification of these global wave modes in VMC data. Also it remains an interesting question whether the irregularly detected mid latitude jets are indeed variable with time or simply become, in parts or in total, shielded from view by higher H_2SO_4 haze layers for varying time intervals.

[55] Winds at latitudes higher than 60°S are still difficult to track because of low contrast and scarcity of features, but increasing data is being collected. Over all, it was possible to extend latitudinal coverage of the cloud top winds with VMC observations.

[56] A first analysis indicated that diurnal and semidiurnal thermal tide modes appear to be present in the data, but a more profound confirmation still depends on synthesis of VIRTIS and VMC observations on night and dayside in order to bridge the large data gap in local time coverage of the VMC UV data between 17 and 9 h local solar time.

[57] Although poorly resolved, results on average meridional wind speed components are in general agreement with previous observations and with the presence of a Hadley cell spanning between equatorial region and about 45°S latitude. Since measurement accuracy is very low so far, so we decided not to use the results on meridional winds for detailed investigations. We expect future data to improve the accuracy up to a degree that allows for more reliable meridional profiles fit for being used to draw more conclusions.

[58] As VMC continues to acquire data, not only more UV data will become available for dayside cloud top level tracking purposes. In addition we are investigating whether data from the two IR channels of the instrument could be used for tracking lower-level features on the day side and extend cloud tracking to the night side. Although contrasts range only from ~1–5% for the IR features in day side images, it might be feasible to improve contrasts through carefully applied filtering processes. Tracking on the night side would prove even more difficult, since VMC is registering signals from the surface simultaneously with those from the lower cloud levels. Efforts for both tracking possibilities are in progress at the moment and will be presented in future works.

[59] Meanwhile operations are increasingly adapted and custom fitted for wind tracking in the UV channel, improving steadily on sequence length and also on timing between individual images. Furthermore wind tracking sequences are extended down to lower altitudes above the planet to allow for higher resolutions and more accurate tracking. One method to achieve this goal is to follow cloud features to compensate for the small area covered by pericenter observations. We hope to achieve tracking sequences with resolutions as high as about 7 km/pixel.

[60] **Acknowledgments.** We would like to thank A. Sanchez-Lavega and R. Hueso for their valuable cooperation and making their latest wind tracking results available to comparison for us. Thanks also go to the International Max Planck Research School on Physical Processes in the Solar System and beyond, the rest of the VMC team for making this work possible, and to NASA for contributions to this paper from grants NNG06GC68G and NNX07AF27G.

References

Belton, M. J. S., P. J. Gierasch, M. D. Smith, P. Helfenstein, P. J. Schinder, J. B. Pollack, K. Rages, D. Morrison, K. P. Klaasen, and C. B. Pilcher (1991), Images from Galileo of the Venus cloud deck, *Science*, *253*, 1531–1536, doi:10.1126/science.253.5027.1531.

Boyer, C., and P. Guerin (1969), Étude de la rotation rétrograde, en 4 jours, de la couche extérieure nuageuse de Vénus, *Icarus*, *11*, 338–355, doi:10.1016/0019-1035(69)90067-0.

Carlson, R. W., et al. (1991), Galileo infrared imaging spectroscopy measurements at Venus, *Science*, *253*, 1541–1548, doi:10.1126/science.253.5027.1541.

Crisp, D., S. McMuldroch, S. K. Stephens, W. M. Sinton, B. Ragent, K.-H. Hodapp, R. G. Probst, L. R. Doyle, D. A. Allen, and J. Elias (1991), Ground-based near-infrared imaging observations of Venus during the Galileo encounter, *Science*, *253*, 1538–1541, doi:10.1126/science.253.5027.1538.

Del Genio, A. D., and W. B. Rossow (1990), Planetary-scale waves and the cyclic nature of cloud top dynamics on Venus, *J. Atmos. Sci.*, *47*, 293–318, doi:10.1175/1520-0469(1990)047<0293:PSWATC>2.0.CO;2.

Gierasch, P., et al. (1997), The general circulation of the Venus atmosphere: An assessment, in *Venus II*, edited by Stephen W. Bougher, D. M. Hunten, and R. J. Philips, pp. 459–500, Univ. of Ariz. Press, Tucson, Ariz.

Kawabata, K., D. L. Coffeen, J. E. Hansen, W. A. Lane, M. Sato, and L. D. Travis (1980), Cloud and haze properties from Pioneer Venus polarimetry, *J. Geophys. Res.*, *85*, 8129–8140, doi:10.1029/JA085iA13p08129.

Limaye, S. S. (1985), Venus atmospheric circulation: Observations and implications of the thermal structure, *Adv. Space Res.*, *5*(9), 51–62, doi:10.1016/0273-1177(85)90270-4.

Limaye, S. S. (1988), Venus: Cloud level circulation during 1982 as determined from the Pioneer Cloud Photopolarimeter images. Part II. Solar longitude dependent circulation, *Icarus*, *73*, 212–226, doi:10.1016/0019-1035(88)90094-2.

Limaye, S. S. (2007), Venus atmospheric circulation: Known and unknown, *J. Geophys. Res.*, *112*, E04S09, doi:10.1029/2006JE002814.

Limaye, S. S., and V. E. Suomi (1981), Cloud motions on Venus: Global structure and organization, *J. Atmos. Sci.*, *38*, 1220–1235, doi:10.1175/1520-0469(1981)038<1220:CMOVGS>2.0.CO;2.

Limaye, S. S., C. J. Grund, and S. P. Burre (1982), Zonal mean circulation at the cloud level of Venus: Spring and fall 1979 OCPP observations, *Icarus*, *51*, 416–439, doi:10.1016/0019-1035(82)90092-6.

Limaye, S. S., C. Grassotti, and M. J. Kuetemeyer (1988), Venus: Cloud level circulation during 1982 as determined from the Pioneer Cloud Photopolarimeter images. Part I. Time and zonally averaged circulation, *Icarus*, *73*, 193–211.

Markiewicz, W. J., et al. (2007a), Venus Monitoring Camera for Venus Express, *Planet. Space Sci.*, *55*(12), 1701–1711, doi:10.1016/j.pss.2007.01.004.

Markiewicz, W. J., D. V. Titov, S. S. Limaye, H. U. Keller, N. Ignatiev, R. Jaumann, N. Thomas, H. Michalik, R. Moissl, and P. Russo (2007b), Morphology and dynamics of the upper cloud layer of Venus, *Nature*, *450*, 633–636, doi:10.1038/nature06320.

Peralta, J., R. Hueso, and A. Sanchez-Lavega (2007), A reanalysis of Venus winds at two cloud levels from Galileo SSI images, *Icarus*, *190*, 469–477, doi:10.1016/j.icarus.2007.03.028.

Piccialli, A., D. V. Titov, D. Grassi, I. A. Khatuntsev, P. Drossart, G. Piccioni, and A. Migliorini (2008), Cyclostrophic winds from the VIRTIS temperature sounding: A preliminary analysis, *J. Geophys. Res.*, *113*, E00B11, doi:10.1029/2008JE003127.

Rossow, W. B., A. D. Del Genio, S. S. Limaye, L. D. Travis, and P. H. Stone (1980), Cloud morphology and motions from Pioneer-Venus images, *J. Geophys. Res.*, *85*, 8107–8128, doi:10.1029/JA085iA13p08107.

Rossow, W. B., A. D. Del Genio, and T. Eichler (1990), Cloud-tracked winds from Pioneer Venus OCPP images, *J. Atmos. Sci.*, *47*, 2053–2084, doi:10.1175/1520-0469(1990)047<2053:CTWFVO>2.0.CO;2.

Sánchez-Lavega, A., et al. (2008), Variable winds on Venus mapped in three dimensions, *Geophys. Res. Lett.*, *35*, L13204, doi:10.1029/2008GL033817.

Schubert, G. (1983), General circulation and the dynamical state of the Venus atmosphere, in *Venus*, edited by D. Hunten, L. Colin, T. Donahue, and V. Moroz, pp. 651–765, Univ. of Ariz. Press, Tucson, Ariz.

Schubert, G., S. W. Bougher, C. C. Covey, A. D. Del Genio, A. S. Grossman, J. L. Hollingsworth, S. S. Limaye, and R. E. Young (2007), Venus atmosphere dynamics: A continuing enigma, in *Exploring Venus as terrestrial planet*, *Geophys. Monogr. Ser.*, vol. 176, edited by L. W. Esposito, E. R. Stofan, and T. E. Cravens, pp. 121–138, AGU, Washington, D. C.

Smith, M. D., and P. J. Gierasch (1996), Global-scale winds at the Venus cloud top inferred from cloud streak orientations, *Icarus*, *123*(2), 313–323, doi:10.1006/icar.1996.0160.

Suomi, V. E. (1975), Cloud motions on Venus, in *The Atmosphere of Venus*, edited by J. E. Hansen, 42 pp., NASA, Washington, D. C.

Svedhem, H., et al. (2007), Venus Express—The first European mission to Venus, *Planet. Space Sci.*, *55*(12), 1636–1652, doi:10.1016/j.pss.2007.01.013.

Titov, D. V., et al. (2006), Venus Express science planning, *Planet. Space Sci.*, *54*(13–14), 1279–1297, doi:10.1016/j.pss.2006.04.017.

Toigo, A., P. J. Gierasch, and M. D. Smith (1994), High resolution cloud feature tracking on Venus by Galileo, *Icarus*, *109*(2), 318–336, doi:10.1006/icar.1994.1097.

Tomasko, M. G., L. R. Doose, and P. H. Smith (1985), The absorption of solar energy and the heating rate in the atmosphere of Venus, *Adv. Space Res.*, *5*(9), 71–79, doi:10.1016/0273-1177(85)90272-8.

M. Almeida, European Space Astronomy Centre, European Space Agency, P.O. Box - Apartado de Correos 78, E-28691 Madrid, Spain.

T. Behnke, R. Jaumann, K.-D. Matz, and T. Roatsch, Institut fur Planetenforschung, Deutsches Zentrum fur Luft- und Raumfahrt, Rutherfordstrasse 2, D-12489 Berlin, Germany.

S. F. Hviid, W. J. Markiewicz, R. Moissl, G. Portyankina, and D. V. Titov, Max-Planck-Institut fuer Sonnensystemforschung, Max-Planck-Strasse 2, D-37191 Katlenburg-Lindau, Germany. (moissl@mps.mpg.de)

N. I. Ignatiev and I. Khatuntsev, Space Research Institute, 84/32 Profsoyuznaya Street, Moscow 117997, Russia.

S. S. Limaye, Space Science and Engineering Center, University of Wisconsin-Madison, 1017 Atmospheric Oceanic and Space Sciences Building, 1225 West Dayton Street, Madison, WI 53706, USA.